PHYSICAL REVIEW B VOLUME 54, NUMBER 17 1 NOVEMBER 1996-I

Raman studies between 11 and 300 K of the effects of Nd additive in ferroelectric lead-titanate ceramics

J. Frantti* and V. Lantto
Microelectronics and Material Physics Laboratories, University of Oulu, P.O. Box 400, 90571 Oulu, Finland

(Received 3 April 1996; revised manuscript received 1 July 1996)

Low-temperature Raman spectroscopy between 11 K and room temperature was used together with room-temperature x-ray-diffraction experiments for a study of the effects of Nd additive in ferroelectric lead-titanate ceramics. Raman spectra were measured between 40 and 1200 cm^{-1} at different low temperatures from ceramic $\mathrm{Pb}_{1-3y/2}\mathrm{Nd}_y\mathrm{TiO}_3$ samples with Nd concentration y between 0 and 10 %. Nd addition was found to decrease strongly the tetragonal strain (c/a ratio at room temperature decreased from 1.064 to 1.034 in the Nd concentration range y from 0 to 10 %) and unit-cell volume (2.0% shrinkage at $y=10\%$) of ferroelectric lead titanate. A frequency decrease of all transverse Raman modes, except the $E(3\mathrm{TO})$ mode, followed the decrease of the tetragonal strain with Nd addition. A quadratic extrapolation of the frequency behavior of $E(1\mathrm{TO})$ and $A_1(1\mathrm{TO})$ modes with Nd concentration y interpreted that the modes become unstable at around $y=30\%$. Our results revealed a subpeak structure for $A_1(1\mathrm{TO})$-mode frequencies in agreement with earlier findings [Foster *et al.*, Phys. Rev. B **48**, 10 160 (1993)]. Nd addition had a strong effect on the relative intensities between different subpeaks. It was also possible to find, on the basis of some earlier computational results, an anharmonic double-well potential energy for $A_1(1\mathrm{TO})$-mode vibrations to fit approximately the observed subpeak frequencies. Some extra unknown Raman peaks were also found to increase with increasing Nd concentration and decreasing temperature. [S0163-1829(96)04642-5]

I. INTRODUCTION

Solid solutions of PbTiO_3 and PbZrO_3 (PZT's) with a perovskite structure are technologically the most important ferroelectrics. Extensive tuning of properties by composition modification is always present with PZT's. The delicate balance in lead titanate of short-range forces favoring the paraelectric cubic phase and long-range Coulomb forces favoring the ferroelectric phase makes the ferroelectric properties sensitive to defects that modify the short-range interactions and to carriers that screen the long-range Coulomb field.[1] Trivalent lanthanide additives like La and Nd are the usual additives in PZT's which are used to modify many properties, such as Curie temperature, conductivity, coercitivity, and compliance. Lead titanate has been studied intensively during the last 25 years, especially in the form of single crystals,[2–5] and it serves as a starting point to understand the effects of different additives and properties of more complex systems like solid solutions of PZT's. Ceramic samples have been mainly used in the study of PZT's, since it is difficult to produce large enough single crystals. In the characterization of different PZT thin and thick films, the material is also polycrystalline.[6,7] Therefore, ceramic PbTiO_3-based samples were used in this study.

Low-temperature Raman spectroscopy was used to study the effects of Nd additive in ferroelectric PbTiO_3 ceramics. Raman spectra were measured between 40 and 1200 cm^{-1} at different low temperatures from ceramic samples cooled (down to 11 K) in a cryostat. $\mathrm{Pb}_{1-3y/2}\mathrm{Nd}_y\mathrm{TiO}_3$ samples contained different amount of Nd with y between 0 and 10 %. The ceramic form has some advantages and disadvantages for the Raman study. For instance, all Raman-active modes can be recorded together in the same spectrum without any geometrical arrangements concerning the crystal orientation with respect to the direction of the propagation and polarization vectors of the light. Raman peaks from ceramic samples coincide with the frequencies from corresponding normal modes propagating along the principal axis.[8] However, the half width at half magnitude (HWHM) values of the Raman peaks from ceramic samples are larger than those measured from single crystals and the powder form may also strengthen the appearance of second-order Raman peaks in the spectra.[8] In PbTiO_3, however, second-order Raman processes display intensities much smaller than those in other isomorphous $AB\mathrm{O}_3$ compounds, which may relate to the low oxygen polarizability in PbTiO_3.[4] The overlapping of Raman peaks with large HWHM values may cause some difficulties for the interpretation of peak parameters (position, integrated intensity and HWHM value) in the Raman spectra. In addition to Raman spectroscopy, x-ray diffraction was also used to study the behavior of lattice constants and unit-cell volume with Nd concentration in PbTiO_3. A volume shrinkage follows Nd addition and makes possible to study the ferroelectric behavior in PbTiO_3 with decreasing unit-cell volume (pressure effect). Cohen[1] has reported results of electronic-structure calculations on BaTiO_3 and PbTiO_3, and demonstrates that hybridization between the Ti $3d$ states and O $2p$ states is essential for ferroelectricity. In the calculations Cohen used the all-electron, full-potential, linearized augmented plane-wave method within the local-density approximation for the exchange and correlation interactions between electrons. The calculations discovered the different ferroelectric phase behavior of the two materials. In PbTiO_3, the lead and oxygen states hybridize, leading to a large strain that stabilizes the tetragonal phase, whereas in BaTiO_3 the interaction between barium and oxygen is completely ionic, favoring a trigonal structure.[1] We use the results of the

0163-1829/96/54(17)/12139(12)/$10.00

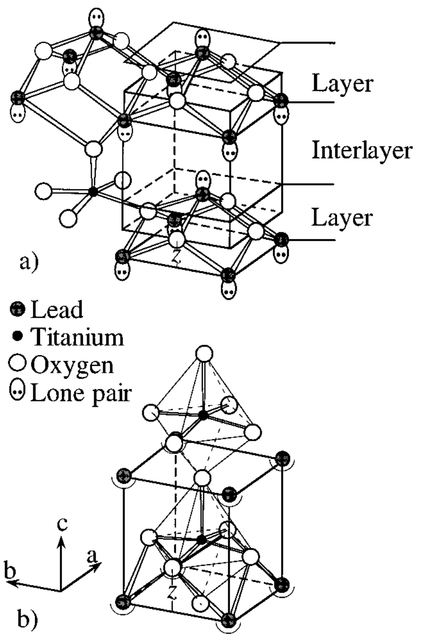

FIG. 1. (a) A solid solution of $(PbO)_{2-x}(TiO_2)_x$ obtained from the α-PbO phase by substituting a TiO_2 group for a Pb*OL* group (after Ref. 9). (b) Tetragonal structure of $PbTiO_3$ where semispheres below lead atoms represent electron clouds due to a strong polarization of lead ions. The internal parameter z is also shown for both structures.

electronic-structure calculations[1] as a reference for our discussions of the effects of anharmonic lattice and Nd additives on the measured Raman spectra.

II. STRUCTURE, POLARIZATION, AND PHONON MODES

The red litharge form of lead oxide, the α-PbO phase with a tetragonal structure, can be used to describe the evolvement of the ferroelectric tetragonal phase of $PbTiO_3$ from the synthesis of PbO and TiO_2 (Fig. 1). Recently there has been a renewal of interest in the study of α-PbO as an incommensurate phase at ambient pressure and low temperatures below 208 K has been evidenced.[9] The layer structure of the tetragonal α-PbO phase at room temperature is shown in Fig. 1(a). The structure is a stacking of regular square pyramids with the Pb^{2+} ions located at the apex of four basal oxygen atoms. These PbO_4 polyhedra are connected, and Pb^{2+} ions are on both sides of the oxygen basal plane to form layers orthogonal to the tetragonal c axis. The electronic lone pairs (L) of the Pb^{2+} ions extend parallel to the c axis and occupy the large interlayer distance, with a volumic occupancy equivalent to that of an oxygen atom.[9] At room temperature the lattice constants a and c in α-PbO are 3.98 and 5.03 Å $(c/a=1.26)$ and the layers of lead atoms with a thickness of 2.37 Å are separated by large interlayers (2.66 Å) which are only occupied by the lone pairs.[9] The only internal structure parameter, i.e., the z coordinate of Pb^{2+} is 1.19 Å [Fig. 1(a)], corresponding to the Pb-O bonding length of 2.31 Å and O-O bonding length of 2.81 Å.

In the addition of titanium oxide TiO_2 into the structure of α-PbO, a TiO_2 group can be substituted for a Pb*OL* group, the extra oxygen atom filling the volume of a lone pair L (Ref. 9) as is shown in Fig. 1(a). In the solid solution of $(PbO)_{2-x}(TiO_2)_x$, extra oxygen atoms occupy the volumes of lone pairs in the interlayers, decreasing the thickness of these interlayers. With the value $x=1$, the ferroelectric tetragonal phase of $PbTiO_3$ is obtained. All lead atoms above (or below) the basal oxygen plane in each lead-oxygen layer are substituted by titanium atoms and half of the volumes of lone pairs in the interlayers are occupied by oxygen atoms as is shown in Fig. 1(b). According to electronic-structure calculations in Ref. 1, a clear polarization of the Pb atoms (from hybrid Pb-O states) with a substantial electron density on the side of lone pairs still exists in the ferroelectric $PbTiO_3$ phase [Fig. 1(b)]. At room temperature, tetragonal lattice constants a and c in $PbTiO_3$ are 3.90 and 4.15 Å with $c/a=1.064$.

The paraelectric phase of $PbTiO_3$ above the Curie temperature $T_C=493$ °C is cubic where Ti atoms are contained in octahedral cages of oxygen ions joined corner to corner. That makes large cuboctahedral cages where the Pb ions sit. In the tetragonal phase at room temperature [Fig. 1(b)] the displacements of Ti and O ions relative to the Pb ion at the origin are parallel to the polar c axis 17 and 47 pm, respectively.[10] As in the α-PbO phase, tetragonal $PbTiO_3$ structure contains also regular square pyramids with the Pb^{2+} ions located at the apex of four basal oxygen atoms. At room temperature the distance z of the Pb^{2+} ion from the oxygen basal plane (O-O bonding length 2.76 Å) is 1.61 Å (Pb-O bonding length 2.53 Å), which is 0.42 Å larger than the corresponding z distance in α-PbO.

Phase transitions in ferroelectric perovskites were long considered displacive transitions, characterized by a zone-center soft mode with a vanishing frequency at the phase transition. In a later work,[11] however, an order-disorder model was proposed, in which there are eight sites along eight cube diagonals $\langle 111\rangle$ for low-energy distortions. In $PbTiO_3$, however, the large strain stabilizes the ordered tetragonal phase, but at high temperatures the cubic $PbTiO_3$ phase also has an underlying multiple-well potential surface.[1] The hybridization of the Ti $3d$ states with the O $2p$ states is the origin of the ferroelectricity in the structure. The results in Ref. 1 show a strong hybridization also between Pb $6s$ and O $2p$ states in $PbTiO_3$, which leads to the large strain that stabilizes the tetragonal phase. The results also show an indirect effect on the Ti-O interactions through the Pb-O hybridization. In the perovskite structure of $Pb_{1-3y/2}Nd_yTiO_3$, Nd^{3+} ions replace Pb^{2+} ions in the large eightfold-coordinated cuboctahedral cages. With Nd^{3+}, however, the hybridization with oxygen states is not possible [compare the Ba^{2+} case in $BaTiO_3$ (Ref. 1)].

The ferroelectric $Pb_{1-3y/2}Nd_yTiO_3$ with $y\leqslant 10\%$ has tetragonal crystal structure with the space group C^1_{4v} as the crystal symmetry. Modes in each three T_{1u} in the paraelectric cubic phase split into modes transforming as the irreducible representation $E\oplus A_1$ of the point group C_{4v}, and the nonpolar T_{2u} cubic modes split into modes transforming as $E\oplus B_1$. As in the cubic phase, long-range Coulomb forces split the modes transforming as $E\oplus A_1$ into transverse TO and longitudinal LO components. The following labeling scheme in the tetragonal phase of $PbTiO_3$ was introduced by Burns and Scott[3] for the optical A_1 and E modes arising from the three T_{1u} representations:

$$\begin{array}{llll} A_1(3\mathrm{TO}) & A_1(3\mathrm{LO}) & E(3\mathrm{TO}) & E(3\mathrm{LO}) \\ A_1(2\mathrm{TO}) & A_1(2\mathrm{LO}) & E(2\mathrm{TO}) & E(2\mathrm{LO}), \\ A_1(1\mathrm{TO}) & A_1(1\mathrm{LO}) & E(1\mathrm{TO}) & E(1\mathrm{LO}) \end{array}$$

where the numbers in the parenthesis increase with the increase of the particular mode frequency. LO and TO refer to longitudinal- and transverse-optical modes, respectively. Coulomb-field splitting of the $E \oplus B_1$ modes from T_{2u} is also allowed, but this has not been observed in $\mathrm{PbTiO_3}$.[5] They are labeled as $E \oplus B_1$ or ‘‘silent.’’

III. EXPERIMENTAL

Ceramic samples, produced under completely constant preparation conditions from raw materials through milling, calcination, milling, granulation, pressing, and sintering in the same crucible by Siemens in Germany, were in the form of discs with diameter and thickness of around 13 and 1 mm, respectively (except a disc with $y=8.0\%$ had a thickness of 0.2 mm). The Nd content y in the samples was between 0 and 10% of A cation sites. X-ray diffraction with Cu $K\alpha$ radiation was used to study the room-temperature structure of the samples. The behavior of the tetragonal lattice constants a and c with Nd concentration y in the structure was carefully studied by using a polycrystalline silicon as a calibration standard. Some measurements were also made in order to study the effects of Nd additives on the dielectric and mechanical properties of the samples. Capacitance and radial resonant-frequency measurements from the discs were used to study, respectively, the behavior of the low-frequency dielectric constant and elastic compliance with the Nd concentration in the structure. These results are, however, not included in this report.

Raman shifts were measured using the Jobin-Yvon T-64000 facility with a charge-coupled-device detector and the 514.532 nm line of an $\mathrm{Ar^+}$ laser. A mercury lamp (strong line at 1122.60 $\mathrm{cm^{-1}}$) was used as a calibration standard for Raman peaks. Two different installations were used in Raman measurements. At room temperature, the micro-Raman utility was used to measure Raman spectra at a backscattering configuration. At temperatures below the room temperature, a macrochamber was used in the measurements at an installation where the directions of the incident and scattered light were perpendicular to each other. The power of the laser beam on samples was between 5 and 8 mW with a spot diameter of some tens of micrometers. At low-temperature measurements, the samples were cooled to different temperatures (down to 11 K) in a cryostat using a helium compressor. Temperature was controlled and measured with a microprocessor-based temperature indicator/controller (Scientific Instruments model 5500-1). A silicon diode was used for sensing temperatures inside the cryostat.

IV. RESULTS

A. X-ray-diffraction experiments

Different 2θ angle intervals were used in the recording of x-ray-diffraction patterns. The first interval was between 10° and 80° and an angular velocity of 0.5 deg/min was used in the recording. In the determination of the lattice constants a and c, separate higher 2θ peaks between 80° and 158° were recorded with an angular velocity of 0.125 deg/min and a polycrystalline silicon was used as an internal calibration standard to calculate corrections for the peak positions as a function of the angle 2θ. All the samples had patterns similar to a homogeneous crystal structure consisting only of the ferroelectric tetragonal phase.

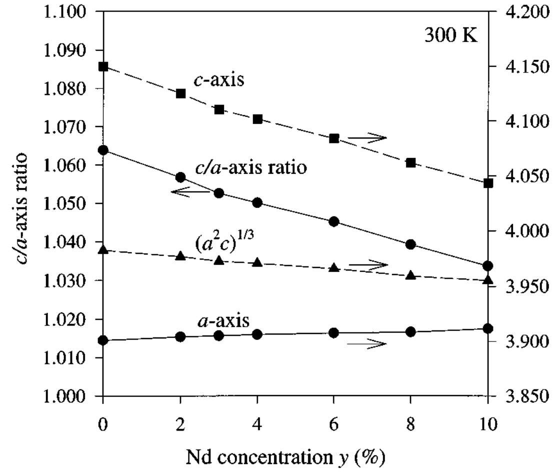

FIG. 2. Lattice constants a and c, the ratio c/a and the cubic root of the unit-cell volume as a function of Nd concentration in $\mathrm{Pb_{1-3y/2}Nd_yTiO_3}$.

A commercial curve-fitting program was used to determine the positions and integrated intensities of different measured x-ray peaks. The following procedure was used to determine the lengths of the lattice constants a and c at room temperature for different samples. The calculated corrections from the silicon reference patterns were added to peak positions obtained from the curve fitting procedure, and the lattice constants a and c were calculated from single peaks of the form $(hk0)$ and $(00l)$, respectively. In the case of (hkl) reflections, the other necessary equation for solving a and c was obtained from the c/a ratio which minimized the value of the sum $\Sigma_i(\overline{a}-a_i)^2$ where both the average lattice constant $\overline{a}$ and the lattice constant a_i, calculated from the ith reflection using Bragg equation and the assumed c/a ratio, depend on the value of the c/a ratio. After plotting of determined a and c values as a function of $\sin^2\theta$, straight lines were fitted to these values and the extrapolated values of a and c at the point $\sin^2\theta=1$ were taken to represent the values of the corresponding lattice constants.

Because of a poling treatment before x-ray-diffraction measurements, the intensity ratios between different x-ray peaks did not correspond to a random grain orientation in Nd-doped samples. In the case of a pure $\mathrm{PbTiO_3}$ sample without any poling, however, the measured intensity ratios were in agreement with the random grain orientation. For instance, the integrated intensity of the higher peak of the {100} (or {200}) twin peaks was nearly twice that of the lower peak [in agreement with the values of the structure factors for (100) and (001) reflections]. The lattice constants a and c, the ratio c/a and the cubic root of the unit-cell volume $(a^2c)^{1/3}$ are shown in Fig. 2 as a function of Nd concentration in $\mathrm{Pb_{1-3y/2}Nd_yTiO_3}$. The strong decrease of the lattice constant c with increasing Nd concentration is the most clear effect of Nd addition. Up to the value $y=10\%$, the lattice constant c decreases by 2.57%, while the lattice con-

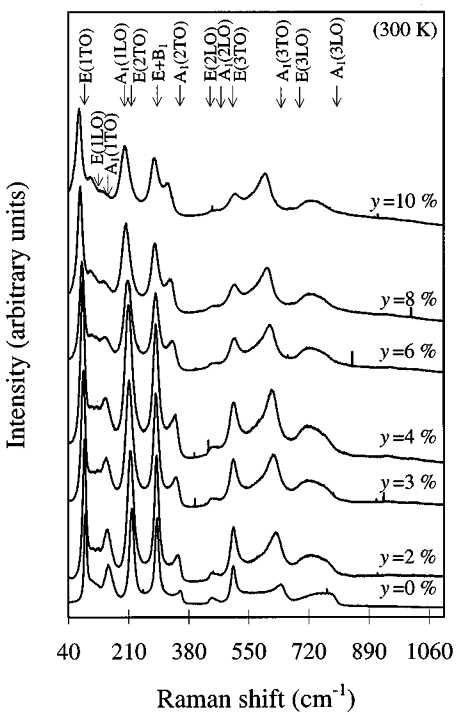

FIG. 3. Raman spectra measured at room temperature from different $Pb_{1-3y/2}Nd_yTiO_3$ samples with y between 0 and 10 %. Positions of different Raman peaks at room temperature in $PbTiO_3$ (Ref. 5) are also shown at the top. There are a few very sharp spikes in the spectra which do not correspond to any real Raman peaks, but probably originate from cosmic rays in the CCD detector.

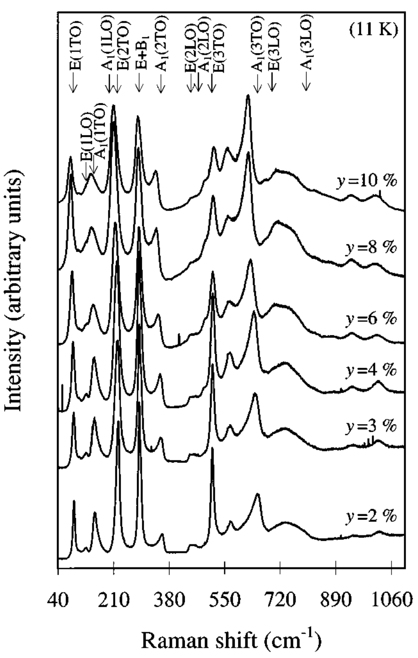

FIG. 4. Raman spectra measured at ambient cryostat temperature of 11 K from different $Pb_{1-3y/2}Nd_yTiO_3$ samples with y between 2 and 10 %. Positions of different Raman peaks at room temperature in $PbTiO_3$ (Ref. 5) are also shown at the top.

stant a increases only by 0.27%. Therefore, a large volume shrinkage follows Nd addition. At $y=10\%$ in Fig. 2, the decrease of the unit-cell volume is about 2.0%.

B. Raman experiments

Figures 3 and 4 show Raman spectra measured from $Pb_{1-3y/2}Nd_yTiO_3$ samples with different y values between 0 and 10 %, respectively, at room temperature and at an ambient cryostat temperature of 11 K. Similar spectra were also measured at ambient temperatures of 100, 150, and 200 K. In addition to the Stokes spectra in Figs. 3 and 4, the corresponding anti-Stokes spectra were also measured at ambient temperatures of 11, 100, 150, 200 K, and room temperature. In order to find the positions, line widths, and intensities of different Raman peaks from the measured spectra, a curve fitting was made for all measured Stokes and anti-Stokes spectra. Voigt, Gauss, and some asymmetric line shapes were used to describe different peak shapes in the spectra. In some cases, however, the determination of peak parameters was practically impossible because of the large overlapping of peaks. Figure 5 shows results of a curve fitting for a spectrum measured from a $Pb_{0.85}Nd_{0.10}TiO_3$ sample at an ambient cryostat temperature of 11 K. Asymmetric line shapes of the modes at 337 cm^{-1} [A_1(2TO)] and 622 cm^{-1} [A_1(3TO)] may originate from oblique phonons (compare with results in Ref. 5).

Figure 6 shows a low-frequency part of the Stokes spectrum in Fig. 5 together with the corresponding anti-Stokes spectrum measured at the same ambient temperature of 11 K. Results of the curve fitting are also shown for both spectra. For a first-order Raman line, the intensity ratio between the anti-Stokes and Stokes lines follows the temperature according to the equation

$$I(\text{anti-Stokes})/I(\text{Stokes}) = \exp(-\hbar\omega/k_BT), \qquad (1)$$

where $\hbar\omega$ is the quantum energy of the phonon. The intensity ratios of the fitted E(2TO) and $E\oplus B_1$ peaks in Fig. 6 gave, respectively, temperatures 84 and 89 K from Eq. (1). The average temperature 86 K is much higher than the ambient temperature 11 K during the measurements in the cryostat. A small-area local phonon excitation and heating by the laser beam is an explanation for this large disparity between the two temperatures. This disparity was found to increase with decreasing ambient temperature in agreement with the strong decrease of the heat capacity according to the Debye cubic law at low temperatures.

Different peak positions obtained from the curve fitting for the spectra in Figs. 3 and 4 are given, respectively, in Tables I and II. In fact, the peak positions in Tables I and II are in most cases average peak positions from the fitted Stokes and anti-Stokes peak positions. The average value may give a higher accuracy for the peak position as compared with the value from a Stokes-peak position alone (accuracy of the order of 1 cm^{-1} in the case of low overlapping between peaks). Average temperatures of two temperature values, calculated according to Eq. (1) from the fitted intensity ratios of anti-Stokes and Stokes lines, respectively, of E(2TO) and $E\oplus B_1$ peaks, are also given for all samples in Tables I and II. The fitting together with the assignment of modes above 400 cm^{-1} in Figs. 3 and 4 (corresponding results in Tables I and II) is uncertain, to some extent. For instance, the unusual shape of the Raman spectrum ($y=0$) in

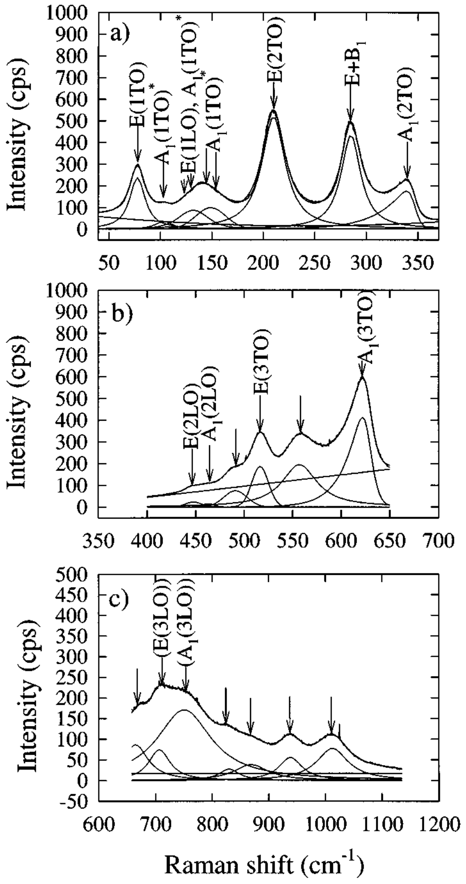

FIG. 5. A Raman spectrum measured at an ambient cryostat temperature of 11 K from a $Pb_{0.85}Nd_{0.10}TiO_3$ sample together with a peak fitting. The labeling of peak positions (* for subpeaks) is also shown (uncertain labels in parenthesis) together with arrows for unknown extra peaks.

Fig. 3 between 500 and 640 cm^{-1} was related to the continuous distribution of oblique modes between E(3TO) and A_1(3TO) (Ref. 5) by Burns and Scott.[8] In all samples with the Nd additive, however, our fitting procedure did interpret an extra unknown mode between the E(3TO) and A_1(3TO) modes in Fig. 3. At low temperatures in Fig. 4, the extra unknown mode is clearly seen at all Nd concentrations y between 2 and 10 %. In the high-frequency range above 650 cm^{-1}, a large overlapping of peaks, e.g., in Fig. 5, makes the interpretation more uncertain. Some new Raman peaks in this frequency range are also seen in Figs. 3, 4, and 5 to increase with increasing Nd concentration and decreasing temperature. Different Raman peaks are seen to broaden with increasing Nd concentration and temperature in Figs. 3 and 4. Figure 7 shows fitted HWHM values at room temperature for the modes E(1TO), E(2TO), and $E \oplus B_1$ as a function of Nd concentration y between 0 and 10 %. The HWHM value of each mode in Fig. 7 increases by about a factor of 2 between Nd concentrations $y=0$ and 10 %.

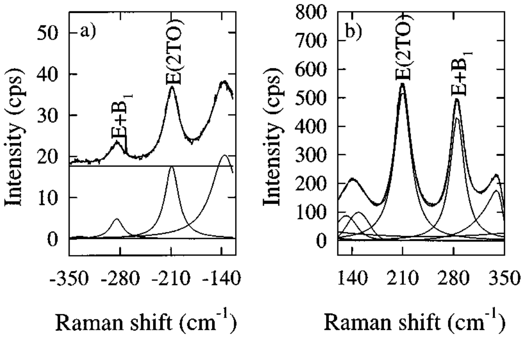

FIG. 6. A low-frequency part of (a) an anti-Stokes and (b) a Stokes spectrum measured at an ambient temperature of 11 K from a $Pb_{0.85}Nd_{0.10}TiO_3$ sample together with a curve fitting for both spectra.

In the low-frequency range of the soft E(1TO) and A_1(1TO) modes, there are large differences in the Raman spectra between different temperatures and samples with different Nd concentrations in Figs. 3 and 4. Especially, this is the case at frequencies above the E(1TO) frequency in Fig. 8 where Raman spectra, measured at three different ambient temperatures from three samples, respectively, with Nd concentrations 2, 6, and 10 %, are shown up to a frequency of 180 cm^{-1}. The temperatures in Fig. 8 refer to average temperatures calculated from the intensity ratios of anti-Stokes and Stokes lines with Eq. (1). Our fitting procedure interprets three different peaks above the E(1TO) frequency for all nine curves in Fig. 8. The fitted relative intensities between the three peaks vary strongly with temperature and Nd concentration in the samples. In pure $PbTiO_3$ at room temperature, the E(1LO) mode has a frequency 128 cm^{-1}, but the mode A_1(1TO) appears as a superposition of four different subpeaks.[5] The four subpeaks of A_1(1TO) frequencies are also marked in Tables I and II. A more detailed discussion for this will be given below.

V. DISCUSSION

For an easy illustration of the behavior of transverse modes with both E and A_1 symmetries (and of the $E \oplus B_1$ peak) with the Nd concentration, we replot in Fig. 9 the frequencies of these modes at room temperature as a function of Nd concentration y from Table I. The frequency of the E(3TO) mode increases with increasing Nd concentration and the frequency of the $E \oplus B_1$ peak is nearly independent of the Nd addition. The frequencies of all other transverse modes in Fig. 9 decrease with increasing Nd concentration. The frequency decrease means a considerable softening of the force constant of the corresponding lattice vibration, since the lighter weight of the Nd atom (144.2), as compared to that of the Pb atom (207.4), has a tendency to increase vibration frequencies. For a more exact consideration of the mode softening, we plotted the squares of the mode frequencies in Fig. 9 as a function of Nd concentration, and fitted a straight line with a quadratic equation

$$\omega(y)^2 = \omega'(0)^2[1\text{-}y/y_0] \tag{2}$$

to the experimental data for each modes. The values of the fitting parameters $\omega'(0)$ and y_0 are given in Table III. In the case of the A_1(1TO) mode, only four $\omega(y)^2$ values of the highest subpeak at $y=0$, 2, 3, and 4 % were used in the fitting, since some inaccuracies may follow at higher Nd concentrations from reasons discussed above and below. The values of the fitting parameter $\omega'(0)$ for all six modes in

TABLE I. Fitted frequencies of different Raman peaks from room-temperature measurements for seven $Pb_{1-3y/2}Nd_yTiO_3$ samples (Fig. 3) together with a labeling of peak positions (uncertain labels in parenthesis). Temperature T_{calc} (in K) refers to an average of two temperatures calculated from the intensity ratios of E(2TO) and $E\oplus B_1$ peaks in Eq. (1) [in the case $y=10\%$, calculated from the intensity ratio of E(2TO) peak alone].

	$y=0\%$ $T_{calc}=247$	$y=2\%$ $T_{calc}=265$	$y=3\%$ $T_{calc}=267$	$y=4\%$ $T_{calc}=258$	$y=6\%$ $T_{calc}=287$	$y=8\%$ $T_{calc}=296$	$y=10\%$ $T_{calc}=330$
E(1TO)	88	85	82	81	77	74	71
subpeak 4	107	106	106	107	105	103	103
E(1LO), subpeak 3	124	123	122	122	120	118	120
A_1(1TO) (subpeaks 1 and 2)	151	148	146	143	141	143	144
E(2TO)	218	214	212	209	207	202	200
$B_1\oplus E$	289	288	287	287	286	284	283
A_1(2TO)	357	349	344	341	334	329	321
E(2LO)	444	447	445	442	444	445	448
A_1(2LO)	458	464	463	456	457	464	476
				472	503	484	480
E(3TO)	504	507	507	507	510	508	509
	532	569	580	592	583	563	561
A_1(3TO)	637	628	621	618	611	603	594
[E(3LO)]	736	703	667	707	664	668	660
[A_1(3LO)]	779	750	719	746	714	718	710
		777	762	772	759	760	742
		824	827	824	823	815	819
		881	881	881	876	876	868
		950	944	946	946	945	945
		1028	1015	1015	1020	1007	1008

Table III are very close to the corresponding experimental frequencies $\omega(0)$ in Table I. At Nd concentration y_0 the frequency $\omega(y_0)$ is zero and the mode becomes unstable. The results in Table III predict that both E(1TO) and A_1(1TO) modes become unstable at around $y=30\%$.

The soft A_1(1TO) and E(1TO) phonons at $\mathbf{k}\approx\mathbf{0}$ in the tetragonal $PbTiO_3$ correspond to vibrations of the lead ion with respect to the slightly distorted TiO_6 octahedra.[12] The displacement polarization is along a and c axes for E(1TO) and A_1(1TO) phonons, respectively. An illustration of the atomic displacements associated with the A_1(1TO) phonon at $\mathbf{k}\approx\mathbf{0}$ is shown in Fig. 10(a). It was found by Foster *et al.*[5] that the anomalous line shape of the A_1(1TO) Raman peak is not a smooth function but appears to be a superposition of four subpeaks at temperatures around room temperature. At 400 K, four distinct subpeaks appeared at 148.5, 137.5, 126.5, and 110.5 cm^{-1}. The four subpeaks were labeled 1, 2, 3, and 4, respectively, in Ref. 5. It was also found that the intensity of peaks 2–4 decreased with decreasing temperature, and the individual peaks become more difficult to resolve. By 60 K, the intensities of peaks 2–4 were found to be so weak that the resulting line shape of A_1(1TO) mode was essentially a single Lorentzian.[5] Our spectra in Fig. 8(a) measured at three different temperatures from a ceramic $Pb_{0.97}Nd_{0.02}TiO_3$ sample are in qualitative agreement with the results in Ref. 5. However, larger peak widths from ceramic samples in Fig. 8 make it impossible to distinguish all four separate subpeaks. The highest peak of the three fitted peaks above the E(1TO) frequency in Fig. 8 is probably a superposition of the subpeaks 1 and 2, while the middle peak is a superposition of the subpeak 3 and E(1LO) peak. Then, the lowest peak of the three fitted peaks in Fig. 8 corresponds to the subpeak 4. In fact, it was possible to distinguish the separate subpeaks 1 and 2 from a spectrum measured at room temperature from a pure ceramic $PbTiO_3$ sample.

Foster *et al.*[5] have proposed a model in which they attribute the anomalous line shape of the A_1(1TO) mode to the anharmonic nature of the effective interatomic potential associated with this phonon. The calculated results in Ref. 1 were used here to test the chances of the proposed model to explain the appearance of the subpeaks in the Raman spectrum. In the tetragonal phase with $c/a=1.06$, the calculated decrease in energy per primitive cell was about 0.22 eV (Ref. 1) for an experimental distortion where the distorted oxygen octahedra is displaced 47 pm relative to lead [A_1(1TO) mode] and Ti is displaced 30 pm (47–17 pm) relative to oxygen [A_1(2TO) mode]. It is possible to divide, with a crude extrapolation of the results in Ref. 1, the total energy decrease of 0.22 eV approximately to 0.08 and 0.14 eV for A_1(1TO) and A_1(2TO) mode distortions, respectively. For a more rigorous treatment of the two distortions, the double-well potential energy $\phi(Q)$ for the normal-mode coordinate Q is described in the form[13]

$$\phi(Q)=\frac{\widetilde{k}_s}{2}Q^2+\frac{\xi}{4}Q^4+\frac{\zeta}{6}Q^6. \tag{3}$$

TABLE II. Fitted frequencies of different Raman peaks from measurements at an ambient temperature of 11 K for six $Pb_{1-3y/2}Nd_yTiO_3$ samples (Fig. 4) together with a labeling of peak positions (uncertain labels in parenthesis). Temperature T_{calc} (in K) refers to an average of two temperatures calculated from the intensity ratios of E(2TO) and $E \oplus B_1$ peaks in Eq. (1).

	$y=2\%$ $T_{calc}=76$	$y=3\%$ $T_{calc}=82$	$y=4\%$ $T_{calc}=94$	$y=6\%$ $T_{calc}=133$	$y=8\%$ $T_{calc}=149$	$y=10\%$ $T_{calc}=86$
E(1TO)	90	91	86	83	80	81
subpeak 4	107	105	105	107	102	103
E(1LO), subpeak 3	125	126	126	123	126	132
A_1(1TO) (subpeaks 1 and 2)	153	151	150	147	146	149
E(2TO)	223	221	219	215	210	209
$B_1 \oplus E$	289	290	288	288	286	285
A_1(2TO)	359	356	353	347	341	338
E(2LO)	447	443	444	446	446	448
[A_1(2LO)]	463	455	455	462	466	463
		483	485	488	491	491
E(3TO)	513	513	514	514	514	517
	567	565	565	563	559	557
A_1(3TO)	652	644	640	630	622	622
	692	694	697	664	667	665
[E(3LO)]	737	735	739	702	706	707
[A_1(3LO)]	771	766	777	755	757	751
	795	794	819	830	831	830
	886	883	884	879	875	869
	946	941	940	940	939	937
	1022	1020	1021	1017	1013	1013

In the case of the A_1(1TO) mode, Q is the displacement of the distorted oxygen octahedra relative to Pb. The three coefficients $\widetilde{k}_s$, ξ and ζ were fitted to give the depth 0.08 eV for the potential energy at the side minimums $Q=\pm 47$ pm and the experimental frequency 149 cm^{-1} for the 1–0 transition of A_1(1TO) mode vibrations at these side minimums. A reduced mass $\mu_{1TO}=65.58$ a.u. ($m_1=m_{Pb}$ and $m_2=m_{Ti}+3m_O$) was used in the calculation of this frequency at the side minimums. The fitted form of the double-well potential for the A_1(1TO) mode is shown in Fig. 10(b), and subpeak frequencies up to $n=4$, calculated from this potential energy by a numerical solution of the Schrödinger equation, are given in Table IV. Results from perturbation calculations up to second order were inaccurate, especially at higher n values. The differences in eigenvalues E_ν between symmetric and antisymmetric wave functions were less than 1 cm^{-1} up to $\nu=4$.

The Morse potential energy from molecule vibrations[14]

$$\phi(Q)=D_e[1-\exp(-aQ)]^2 \tag{4}$$

can also be used instead of Eq. (3) to describe the anharmonic nature of the effective interatomic potential energy. D_e is the depth of the potential energy minimum and $a=(k/2D_e)^{1/2}$ where k is the harmonic force constant at the minimum energy. The Schrödinger equation can be solved exactly for this potential energy, the eigenvalues being

$$E_\nu=(\nu+\tfrac{1}{2})\hbar\omega-(\nu+\tfrac{1}{2})^2\hbar\omega x; \quad \nu=0,1,2,\ldots, \tag{5}$$

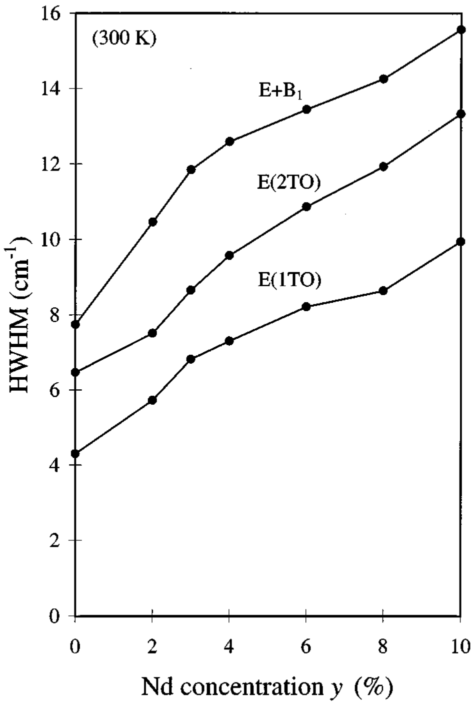

FIG. 7. Fitted HWHM values from Raman spectra in Fig. 3 for E(1TO), E(2TO), and $E \oplus B_1$ peaks as a function of Nd concentration y between 0 and 10 %.

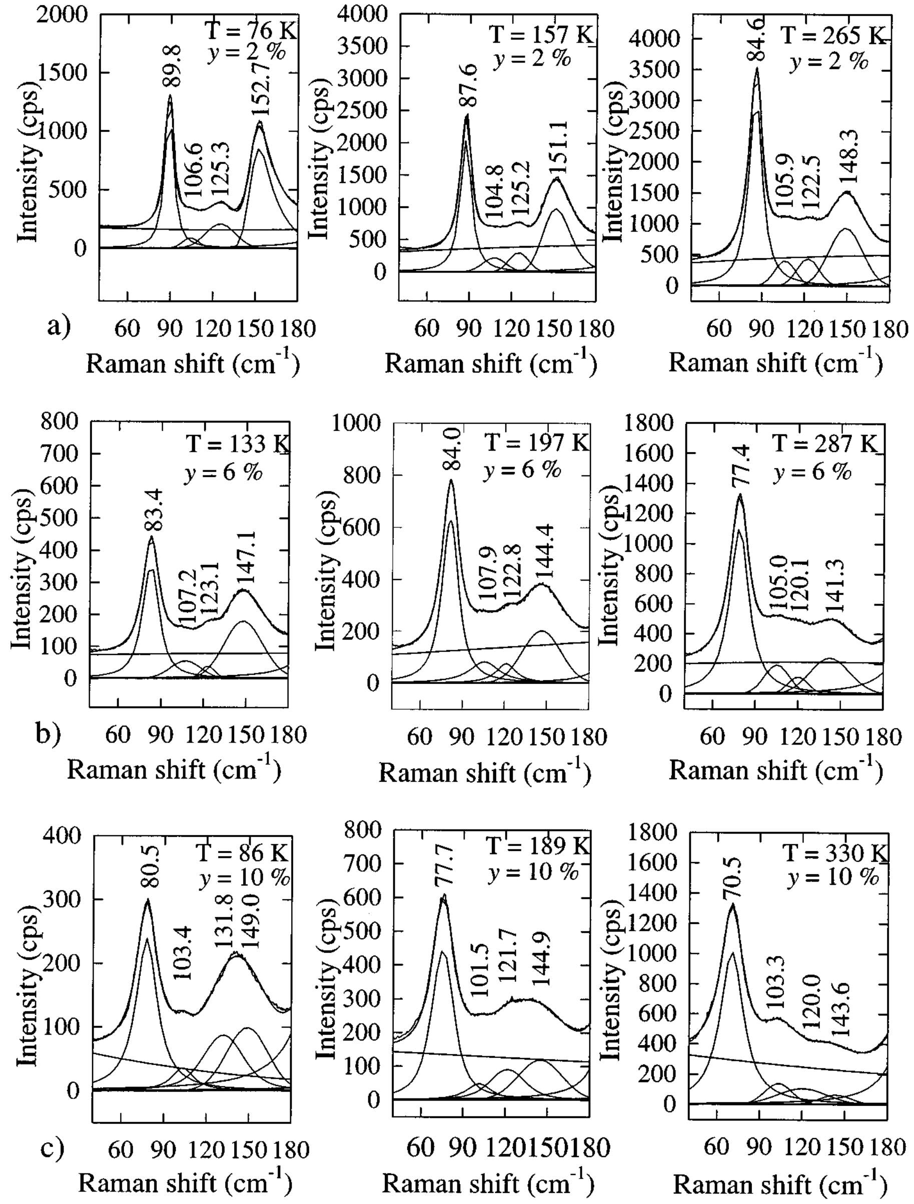

FIG. 8. Low-frequency Raman spectra measured at three different ambient temperatures (11, 150 K, and room temperature) from $Pb_{1-3y/2}Nd_yTiO_3$ samples with (a) $y=2\%$, (b) $y=6\%$, (c) $y=10\%$ together with a peak fitting for all nine spectra. Temperature values in the figures refer to temperatures calculated from Eq. (1) (compare Tables I and II).

with $\omega=(k/\mu)^{1/2}$ and $x=\hbar a^2/2\mu\omega$. The same fitting as above for Eq. (3) was also used for the Morse potential energy [Fig. 10(b)], and corresponding subpeak frequencies, calculated from Eq. (5), are given in Table IV. The subpeak frequencies from the fitting of Eq. (3), however, are closer to the experimental frequencies in the table.

An increase of D_e in the Morse potential energy Eq. (4) from 0.089 to 0.127 eV fitted also the frequency of the subpeak 4 with the experimental frequency 111 cm^{-1}, as shown in Table IV. All four calculated subpeak frequencies in Table IV are now close to the experimental values. A well depth of about 0.1 eV instead of 0.08 eV in the fitting of the potential energy Eq. (3) [Fig. 10(b)] moves also all four calculated subpeak frequencies close to the experimental values in Table IV.

In the anharmonic potential model for subpeaks, the intensity of a given transition is proportional to the population of the initial state, and statistics can be used to predict the relative intensities of different subpeaks at different temperatures. The relative intensity R of the Stokes transition from level $n+1$ to n to that of the 1 to 0 transition was given in Ref. 5 by the equation

$$R=(n+1)\exp[-n\hbar\omega/(k_BT)], \tag{6}$$

where for the A_1(1TO) mode in pure $PbTiO_3$, $\hbar\omega$ is 149 cm^{-1}=213 K at room temperature. In samples with low Nd concentration [pure $PbTiO_3$ and the sample in Fig. 8(a) with $y=2\%$], the fitted relative intensities of subpeaks are in qualitative agreement with Eq. (6) at higher temperatures. For instance, the intensity of the fourth subpeak at room temperature in Fig. 8(a) is about one fourth of the intensity of the highest peak (superposition of subpeaks 1 and 2) in close agreement with Eq. (6). The increasing discrepancy between fitted intensities and Eq. (6) with decreasing temperature may relate to the excitation of phonons by the laser beam (interpretation of temperature from the intensity ratio between anti-Stokes and Stokes lines). The discrepancy be-

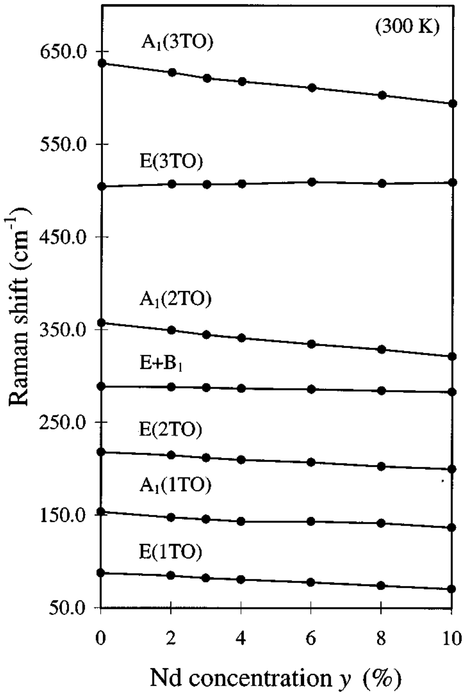

FIG. 9. Frequencies of different transverse modes (and of the $E\oplus B_1$ peak) from Table I as a function of Nd concentration. A_1(1TO) frequencies are highest subpeak frequencies.

tween experimental results and Eq. (6) increases very strongly with increasing Nd concentration in Figs. 8(b) and 8(c).

Fontana *et al.*[4] conclude from their computed components of the effective charge of lead ions in $PbTiO_3$ that the bonds between lead and oxygen in tetragonal $PbTiO_3$ are mainly covalent and ionic, respectively, for directions parallel and normal to the polar *c* axis. It was possible to conclude[15] from the high sensitivity of the E(1TO)-mode frequency on the Zr concentration in PZT that the addition of Zr softens strongly the ''ionic'' force constant of vibrations with displacement polarization in the direction of the *a* axis. For A_1(1TO)-mode vibrations with polarization in the direction of the *c* axis, the force constant, originating from mainly covalent bonding between lead and oxygen, was found to be insensitive to Zr addition.[15] In the case of Nd addition, it is possible to see in Fig. 9 that the frequencies of E(1TO) and A_1(1TO) (the highest subpeak) modes decrease by about the same slope with increasing Nd concentration and a quadratic extrapolation [Eq. (2)] interprets that both modes become unstable at around $y=30\%$. The form of the fitted potential energy in Fig. 10(b) shows that the force constant of A_1(1TO)-mode vibrations decreases with decreasing c/a ratio. This explains the softening of the A_1(1TO) mode in Fig. 9 with increasing Nd concentration (Fig. 2). The softening of the E(1TO) mode with increasing Nd concentration in Fig. 9 may relate to the decrease of the electronic polarization of Pb ions [Fig. 1(b)] with decreasing ferroelectric distortion,[1] which follows the Nd addition. The increase of the lattice constant *a* with Nd addition (Fig. 2) may also have a similar effect on the E(1TO)-phonon frequency. The second transverse phonons 2TO in both E and A_1 symmetries consist of displacements of the Ti ion relative to oxygen ions with the displacement polarization along *a* and *c* axes, respectively. In the tetragonal phase of $PbTiO_3$, Ti strongly distorts with respect to oxygen (30 pm) and bonds with the closer oxygen (filling the volume of the lone pair in Fig. 1).[4] Therefore, the force constant for A_1(2TO)-mode vibrations originates also from a covalent bonding and the force constant for E(2TO)-mode vibrations has an ionic character. It was possible to obtain potential energy values for the A_1(2TO)-mode at four distortion values Q by subtracting the potential energy in Fig. 10(b) from the calculated energy values of the experimental distortion in Ref. 1. After a fitting of Eq. (3) through these four values, a numerical solution of the Schrödinger equation with the fitted potential energy and reduced mass

TABLE III. Values of $\omega'(0)$ and y_0 in Eq. (2) from a fitting to room-temperature frequencies in Fig. 9 for E(1TO), A_1(1TO), E(2TO), $E\oplus B_1$, A_1(2TO), and A_1(3TO) modes.

Normal mode	$\omega'(0)$ (cm^{-1})	y_0 (%)
E(1TO)	87	28.3
A_1(1TO)	153	32.2
E(2TO)	217	61.7
$E\oplus B_1$	289	(245.3)
A_1(2TO)	356	53.0
A_1(3TO)	635	78.9

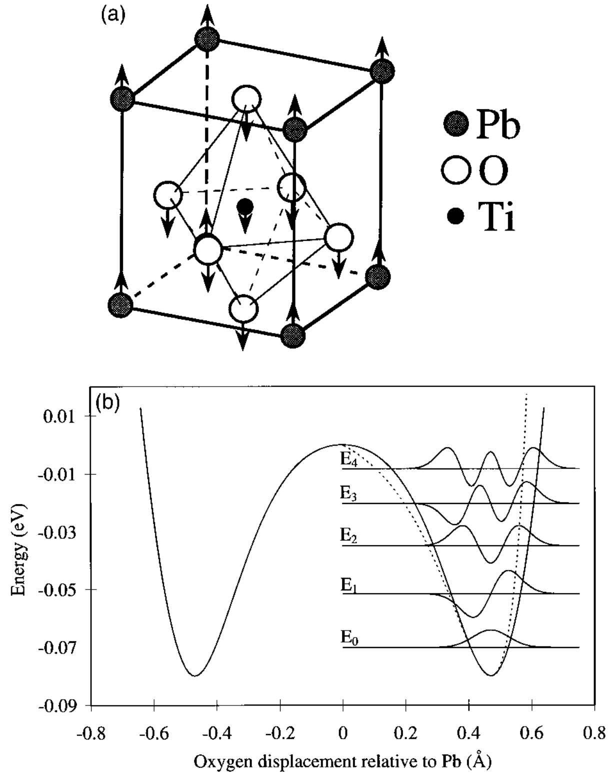

FIG. 10. (a) Relative displacements of lead, oxygen and titanium ions in the optical A_1(1TO) mode in $PbTiO_3$. (b) Double-well potential energy of the A_1(1TO) mode fitted with Eq. (3) (—) together with the corresponding energy levels E_v and harmonic wave functions ψ_v^0 up to $v=4$ to illustrate the insufficiency of the perturbation approach. The dotted line shows a fitted Morse potential energy with $D_e=0.089$ eV in Eq. (4).

TABLE IV. Calculated frequencies of subpeaks n (transition n—$n-1$) up to $n=4$ for A_1(1TO) and A_1(2TO) modes from potential energies fitted with Eqs. (3) and (4) (Morse potential). Experimental frequencies for the A_1(1TO) mode refer to results at 400 K in Ref. 5.

	A_1(1TO)				A_1(2TO)	
n	Experimental frequencies (Ref. 5) (cm^{-1})	Numerical solutions of Eq. (3) (cm^{-1})	Morse potential with $D_e=0.089$ eV (cm^{-1})	Morse potential with $D_e=0.127$ eV (cm^{-1})	Numerical solutions of Eq. (3) (cm^{-1})	Morse potential with $D_e=0.157$ eV (cm^{-1})
1	149	149	149	149	308	365
2	138	135	129	136	275	286
3	127	118	110	123	233	210
4	111	97	90	111	158	133

$\mu_{2TO}=40.34$ a.u. ($m_1=m_{Ti}$ and $m_2=m_{Pb}+3m_O$) gave a subpeak structure, which is also shown in Table IV. Results for the A_1(2TO) subpeak structure from a similar fitting by the Morse potential energy Eq. (4) are also shown in Table IV. The experimental Raman spectra, however, do not show any subpeak structure for the A_1(2TO) mode. The subpeak frequencies from the fitted Morse potential in Table IV are very near to other Raman peaks in Table I and the frequency 365 cm^{-1} for the 1–0 transition is very near to the experimental frequency 359 cm^{-1} in Table I.

Some extra unknown Raman peaks appear from Nd addition at higher frequencies, and the relative intensities of these peaks increase with decreasing temperature. Therefore, they are not second-order peaks. Two extra peaks around the E(3TO) peak in Figs. 4 and 5 are very clear and their frequencies are 65 and 131 cm^{-1}, respectively, below the A_1(3TO) frequency in Table II. Two clear peaks increase also at frequencies of about 940 and 1020 cm^{-1} with increasing Nd concentration in Fig. 4. These peaks are much weaker at room temperature in Fig. 3. The fitting also reveals two weak peaks between 800 and 900 cm^{-1} (Fig. 5), that also increase with increasing Nd concentration. It is not known, if some extra peaks are an indication of another phase. X-ray-diffraction patterns showed only the tetragonal phase at room temperature.

A volume shrinkage follows the Nd addition as shown in Fig. 2. The results in Ref. 1 also show a large volume dependence of the soft-mode potential surfaces, consistent with the loss of ferroelectricity at high pressures in the titanates. Under volume shrinkage the well depths decrease and finally vanish and there is a tricritical point where the transition changes from first-order to continuous.[1] Calculated distortion energies are shown in Ref. 1 for a case where the unit-cell volume of $PbTiO_3$ shrinks 1.2% from 63.28 to 62.51 Å^3 with a considerable decrease in the well depth. The same volume shrinkage of 1.2% is obtained by the addition of 5% Nd in Fig. 2. A linear extrapolation of the c/a values in Fig. 2 gave a Nd concentration $y=21\%$ for the value $c/a=1$.

Radial resonant-frequency measurements from disc samples make it possible to study the behavior of the elastic compliance of $PbTiO_3$ with the Nd addition, if the density behavior with Nd concentration is known. In addition to the volume shrinkage, the defect structure produced by the Nd addition is important for the density behavior. Our nominal formula $Pb_{1-3/2y}Nd_yTiO_3$ means that Nd^{3+} ions substitute Pb^{2+} ions in A sites and the excess positive charge is compensated by lead vacancies for the maintenance of electrical neutrality. Then, the density of a single-crystal sample decreases with Nd concentration as calculated in Table V (density ρ_1) from the volume shrinkage in Fig. 2. Density values are also calculated in Table V (density ρ_2) for the case where divalent Nd^{2+} ions substitute Pb^{2+} ions in A sites without any vacancy compensation. The density stays now about constant in spite of the volume shrinkage in Fig. 2. The measured density values in Table V reveal some porosity (in addition to open grain boundaries) in our ceramic samples. The results in Table V also show that the porosity decreases with increasing Nd concentration.

Since lanthanum appears as an additive to PZT in so many applications, there are much more reports of defect structures produced by La in $PbTiO_3$ and PLZT's. All the rare earths form large trivalent ions, and La^{3+} is the biggest at 0.106 nm for the ionic radius. The structural properties of Nd are very similar to those of La. Nd^{3+} has also a large ionic radius of 0.0995 nm and the trivalent oxides Nd_2O_3 and La_2O_3 have the same hexagonal (A-type) structure which contains one molecule unit per unit cell. Trivalent oxides with smaller rare-earth ions crystallize in monoclinic (B-type) and cubic (C-type) structures. Divalent oxides LaO and NdO have also the same rocksalt structure. Therefore, it may be possible to assume that the defect structures produced by Nd and La additives in $PbTiO_3$ are very similar, respectively. There are many results[16,17] to confirm that La^{3+} ions substitute Pb^{2+} ions in A sites in $PbTiO_3$ and the vacancy compensation is the main mechanism for the maintenance of electric neutrality. The distribution of the compensating vacancies between A and B sites in the $PbTiO_3$ structure is considered in Refs. 16 and 17. In a later work[18] it has been shown that vacancies at Ti sites are unlikely to occur. However, direct microscopic experimental observations for the configuration

TABLE V. Calculated densities ρ_1 and ρ_2 with different Nd concentrations y, respectively, for Nd^{3+} and Nd^{2+} substitution of Pb^{2+} ions in $PbTiO_3$ single crystals together with the measured densities ρ_m from ceramic samples.

	ρ_1 (kg m^{-3})	ρ_2 (kg m^{-3})	ρ_m (kg m^{-3})
$y=0$	7971	7971	
$y=2\%$	7917	7972	6382
$y=3\%$	7898	7980	6600
$y=4\%$	7866	7976	6643
$y=6\%$	7805	7971	6796
$y=8\%$	7756	7977	6681
$y=10\%$	7689	7967	7062

and distribution of defects are still lacking even in the case of La additives, although some conclusions have been drawn, e.g., from positron lifetime measurements.[19,20]

Burns and Scott[21] have measured Raman spectra from $PbTiO_3$ ceramics containing different amounts of La up to $y=24\%$ of A sites. Their spectra measured at room temperature for the La concentrations $y=5$ and 10 % are very similar to the spectra with corresponding Nd concentrations in Fig. 3, and the shapes of their spectra from samples with La concentrations $y=20$ and 24 % are characteristic to the ferroelectric trigonal phase. It was also found in Ref. 22 that the structure changes at 0 °C to the paraelectric cubic phase at La concentration $y=27\%$. All our x-ray and Raman results up to Nd concentration $y=10\%$ are consistent with the ferroelectric tetragonal phase. The Nd concentration y of about 30%, corresponding to the extrapolation limit for unstable $E(1\mathrm{TO})$ and $A_1(1\mathrm{TO})$ modes, may relate to the disappearance of the ferroelectric state. The ferroelectric tetragonal phase may also change to the trigonal symmetry form at lower Nd concentrations before the ferroelectricity disappears. The extrapolation limit y of about 20% for the value $c/a=1$ in Fig. 2 may relate to this symmetry change in the ferroelectric state. With these interpretations Nd and La additives have very similar effects on the ferroelectric properties of $PbTiO_3$ ceramics. We end our discussion with a short summary of the effects of Nd addition on some dielectric and ferroelectric properties of $PbTiO_3$:

(1) The familiar Lyddane-Sachs-Teller (LST) equation relates the frequencies of the longitudinal- and transverse-optical modes to the dielectric constant $\varepsilon(\infty)$ in the optic region (square of the refractive index) and the zero-frequency clamped dielectric constant $\varepsilon(0)$.[21] In the case of an axial ferroelectric crystal, for ε along the c axis, ε_c, only A_1 symmetry modes appear in the LST equation, and for ε_a, perpendicular to the c axis, the modes transform as the E irreducible representation. Nd addition increases the ionic polarizability of lead titanate because of the strong softening of the $A_1(1\mathrm{TO})$ and $E(1\mathrm{TO})$ modes with increasing Nd concentration. Therefore, the ratios $\varepsilon_c(0)/\varepsilon_c(\infty)$ and $\varepsilon_a(0)/\varepsilon_a(\infty)$ increase with increasing Nd concentration, and the soft-mode frequencies dominate the changes in these ratios. At room temperature, it is possible to calculate from the frequency values in Table I an increase from 17.6 to 24.1 for the ratio $\varepsilon_a(0)/\varepsilon_a(\infty)$ with an increase in Nd concentration y from 0 to 10 %. Our value 17.6 for the case $y=0$ is a little higher than the value 16.1 calculated from single crystal measurements in Ref. 5. At an ambient temperature of 11 K, the frequency values in Table II give an increase from 16.0 to 22.8 for the ratio $\varepsilon_a(0)/\varepsilon_a(\infty)$ when Nd concentration y increases from 2 to 10 %. A similar increase with increasing Nd concentration may also relate to the ratio $\varepsilon_c(0)/\varepsilon_c(\infty)$. The calculations, however, need the frequency of the $A_1(1\mathrm{LO})$ mode that was not possible to reveal from our measured Raman spectra. The ratio $\varepsilon_c(0)/\varepsilon_c(\infty)$ in lead titanate is smaller than the ratio $\varepsilon_a(0)/\varepsilon_a(\infty)$ [e.g., a value 4.3 was calculated at room temperature from single-crystal measurements for the ratio $\varepsilon_c(0)/\varepsilon_c(\infty)$ in Ref. 5]. In the case of La additives in $PbTiO_3$, the values calculated for $\varepsilon(0)$ from the LST equation were found to be smaller than the values obtained from capacitance measurements.[21] Our capacitance measurements showed a similar trend also in the case of Nd additives in $PbTiO_3$. The increase of the $\varepsilon(0)$ value above the LST value was related to a contribution from relaxation modes due to impurities, disorder, and nonstoichiometry in Ref. 21.

(2) Spontaneous polarization P_s decreases together with the spontaneous strain c/a with increasing Nd concentration in $PbTiO_3$. According to an experimental relation $P_s \propto \sqrt{c/a-1}$ in Ref. 3, the decrease of the spontaneous strain in Fig. 2 corresponds to a decrease of 27% for P_s at Nd concentration $y=10\%$. The decrease of $\sqrt{c/a-1}$ from Fig. 2 is much faster than the decrease of the $A_1(1\mathrm{TO})$ mode frequency in Fig. 9 with increasing Nd concentration (compare Ref. 3).

(3) The Curie temperature T_C decreases with increasing Nd concentration in $PbTiO_3$. The behavior of T_C with Nd addition seems to be similar to that of La addition. At a La concentration $y=10\%$, T_C was found to decrease from 493 °C ($y=0$) to about 370 °C in Ref. 21. All Raman modes disappeared from our Raman spectrum measured at 400 °C from the sample with Nd concentration $y=10\%$, and only some broad and weak modes were present in a spectrum measured at 311 °C from the same sample. $E(1\mathrm{TO})$ mode from the sample was found to soften with increasing temperature and disappear under a strong background at about 290 °C. Above this temperature the low-frequency background in the Raman spectrum weakened and at about 380 °C the spectrum had only a few very broad peaks and an essentially weakened low-frequency background.

VI. CONCLUSIONS

Detailed Raman studies have been reported of the optical phonons of lead-titanate ceramics with different Nd-additive concentrations up to 10% of A cation sites. Raman spectra were measured at room temperature and at different low cryostat temperatures down to 11 K. All Raman peaks, characteristic to the ferroelectric tetragonal phase, were found in the Raman spectra of all samples down to the ambient temperature of 11 K. A considerable phonon excitation by laser light, corresponding to a local heating, was possible to deduce at low cryostat temperatures from the values calculated for temperature from intensity ratios between anti-Stokes and Stokes lines [Eq. (1)]. Some extra unknown Raman peaks were also found to increase with increasing Nd concentration and decreasing temperatures. Nd addition had a strong effect on the relative intensities between different $A_1(1\mathrm{TO})$-mode subpeaks, which were revealed by a peak fitting from all measured Raman spectra (Fig. 8). It was also possible to find, on the basis of computational results in Ref. 1, an anharmonic double-well potential energy for $A_1(1\mathrm{TO})$-mode vibrations to fit approximately the observed subpeak structure.[5] The frequency behavior of phonons with Nd concentration in $Pb_{1-3y/2}Nd_yTiO_3$ was found to follow the lattice relaxation with Nd addition. X-ray results showed a strong decrease of the tetragonal strain and unit-cell volume with increasing Nd concentration, and a cubic axis ratio $c/a=1$ was obtained at Nd concentration $y=21\%$ from a linear extrapolation of the measured behavior of the c/a ratio with Nd concentration. The effects of Nd addition to the properties of $PbTiO_3$ ceramics seem to be very similar to those of La addition.

ACKNOWLEDGMENTS

We wish to thank Dr. K. Lubitz for his kind supply of the main part of the samples for this study. J. Levoska is acknowledged for discussions concerning x-ray-diffraction measurements, Dr. T. T. Rantala for help in numerical computations, and T. Murtoniemi and E. Siren for their help in constructing the cooling system. J. F. acknowledges the financial support of the foundation Jenny ja Antti Wihurin rahasto in Finland.

---

*Electronic address: iif@ee.oulu.fi

[1] R. E. Cohen, Nature (London) **358**, 137 (1992).

[2] Gerald Burns and Bruce A. Scott, Phys. Rev. Lett. **25**, 167 (1970).

[3] Gerald Burns and Bruce A. Scott, Phys. Rev. B **7**, 3088 (1973).

[4] M. D. Fontana, H. Idrissi, G. E. Kugel, and K. Wojcik, J. Phys. Condens. Matter. **3**, 8695 (1991).

[5] C. M. Foster, Z. Li, M. Grimsditch, S. K. Chan, and D. J. Lam, Phys. Rev. B **48**, 10 160 (1993).

[6] J. Frantti and V. Lantto, J. Appl. Phys. **76**, 2139 (1994).

[7] J. Frantti, V. Lantto, and J. Lappalainen, Ferroelectrics **184**, 69 (1996).

[8] Gerald Burns and Bruce A. Scott, Phys. Rev. Lett. **25**, 1191 (1970).

[9] D. Bellac, J. M. Kiat, P. Garnier, H. Moudden, Ph. Sciau, P. A. Buffat, and G. André, Phys. Rev. B **52**, 13 184 (1995).

[10] G. Shirane, R. Pepinsky, and B. C. Frazer, Acta Crystallogr. **9**, 131 (1956).

[11] R. Comes, M. Lambert, and A. Guinier, Acta Crystallogr. A **26**, 244 (1970).

[12] J. D. Freire and R. S. Katiyar, Phys. Rev. B **37**, 2074 (1988).

[13] T. Hidaka, J. Phys. Soc. Jpn. **61**, 1054 (1992).

[14] P. W. Atkins, *Molecular Quantum Mechanics*, 2nd ed. (Oxford University Press, Oxford, 1992).

[15] J. Frantti, V. Lantto, and J. Lappalainen, J. Appl. Phys. **79**, 1065 (1996).

[16] D. Hennings and G. Rosenstein, Mater. Res. Bull. **7**, 1505 (1972).

[17] K. H. Härdtl and D. Hennings, J. Amer. Ceram. Soc. **55**, 230 (1972).

[18] K. Keiser, J. Bouwma, and A. S. Burggraaf, Ferroelectrics **7**, 341 (1974).

[19] Yuanjin He, Weizhong Yu, Jiajiong Xiong, and Longtu Li, in *Positron Annihilation*, edited by P. C. Jain, R. M. Singru, and K. P. Gopinathan (World Scientific, Singapore, 1985), p. 687.

[20] C. Q. Tang, Phys. Rev. B **50**, 9774 (1994).

[21] Gerald Burns and B. A. Scott, Solid State Commun. **13**, 417 (1973).

[22] D. Hennings and K. H. Härdtl, Phys. Status Solidi A **3**, 465 (1970).